PERGAMON

Journal of Structural Geology 25 (2003) 469–480

JOURNAL OF STRUCTURAL GEOLOGY

www.elsevier.com/locate/jsg

A deformation apparatus for three-dimensional coaxial deformation and its application to rheologically stratified analogue material

G. Zulauf[a,*], J. Zulauf[a], P. Hastreiter[b], B. Tomandl[b]

[a]*Institut für Geologie und Mineralogie, Universität Erlangen-Nürnberg, Schloβgarten 5, 91054 Erlangen, Germany*
[b]*Neurocenter, Department of Neurosurgery, Universität Erlangen-Nürnberg, Schwabachanlage 6, 91054 Erlangen, Germany*

Accepted 1 February 2002

Abstract

A new apparatus is described that supports all types of three-dimensional coaxial deformation from pure constriction to pure flattening. Up to 78% shortening is possible at strain rates ranging from 4×10^{-6} to 1×10^{-2} s^{-1}. The apparatus has been used to study the influence of the deformation regime on the geometry of a deforming stiff layer embedded in a weak matrix. Layer and matrix consist of plasticine, the apparent viscosity η and stress exponent n of which vary from 2×10^6 to 2×10^7 Pa s and 6–9, respectively. First results suggest a considerable influence of the deformation regime on the geometry of the deformed layer including its thickness. If the viscosity ratio between layer and matrix is small ($\eta_2/\eta_1 \cong 5$), folding is restricted to the flattening and plane strain regime, the latter if the layer is initially oriented perpendicular to the long axis X of the finite strain ellipsoid. If the layer is oriented perpendicular to the intermediate Y axis under plane and constrictional strain, low viscosity ratios result in boudinage, but folding is hardly developed. However, simultaneous growth of folds and boudins is possible under pure constriction at a viscosity ratio of 10. Three-dimensional images, based on computer tomography, suggest a strong interaction between such coeval folds and boudins, resulting in characteristic deformation patterns that should not occur if both structures form in sequence during polyphase deformation.

Keywords: Deformation apparatus; Three-dimensional coaxial deformation; Rheologically stratified analogue material

1. Introduction

Scale modelling using analogues of rock materials, such as plasticine, paraffin wax, silicone putty, or clay, has been commonly used to model geological structures like folds, boudins, mullions, etc. (e.g. Ramberg, 1955, 1961; Biot, 1961; Hudleston, 1973; Strömgård, 1973; Cobbold, 1975a,b; Watkinson, 1975; Neurath and Smith, 1982; Mancktelow, 1988; Sokoutis, 1990; Mandal and Khan, 1991; Abbassi and Mancktelow, 1992; Grujic and Mancktelow, 1995; Kidan and Cosgrove, 1996; Williams and Jiang, 2001). Most of these models imply plane strain conditions, with the length of the intermediate Y axis of the finite strain ellipsoid kept constant. However, the finite strain of many natural tectonites deviates significantly from plane strain (e.g. Pfiffner and Ramsay, 1982). Naturally deformed rocks may consist of L, L > S, S > L, or S tectonites, where the longitudinal strain e along the Y axis deviates from zero. The origin of L and L > S tectonites in particular has been hardly verified by experiments. This is largely due to the difficulties involved in building an appropriate deformation apparatus (e.g. Gapais et al., 1991; Kobberger and Zulauf, 1995). Kobberger and Zulauf (1995) put rheologically stratified plasticine into a shear cylinder made of PVC to produce constrictional folds and boudins. This shear cylinder works well in cases where relatively soft analogue material is used. However, if the specimen is relatively strong (e.g. in the case of mullions where a weak layer is embedded in a stiff matrix), use of the PVC shear cylinder has several important drawbacks. First, the PVC of the shear cylinder is no longer stable resulting in inhomogeneous deformation and/or damage of the cylinder. Second, it is hardly possible to reduce the diameter of the shear cylinder without hydraulic equipment. Because of these shortcomings we designed and built a new apparatus that is not restricted to constriction. This machine can produce the full range of three-dimensional coaxial deformation, from pure constriction via plane strain to pure flattening.6

2. The new deformation apparatus

A technical drawing and photographs of the new apparatus

* Corresponding author. Tel.: +49-9131-85-22617; fax: +49-9131-85-29295.
E-mail address: zulauf@geol.uni-erlangen.de (G. Zulauf).

0191-8141/03/$ - see front matter © 2002 Elsevier Science Ltd. All rights reserved.
PII: S0191-8141(02)00023-8

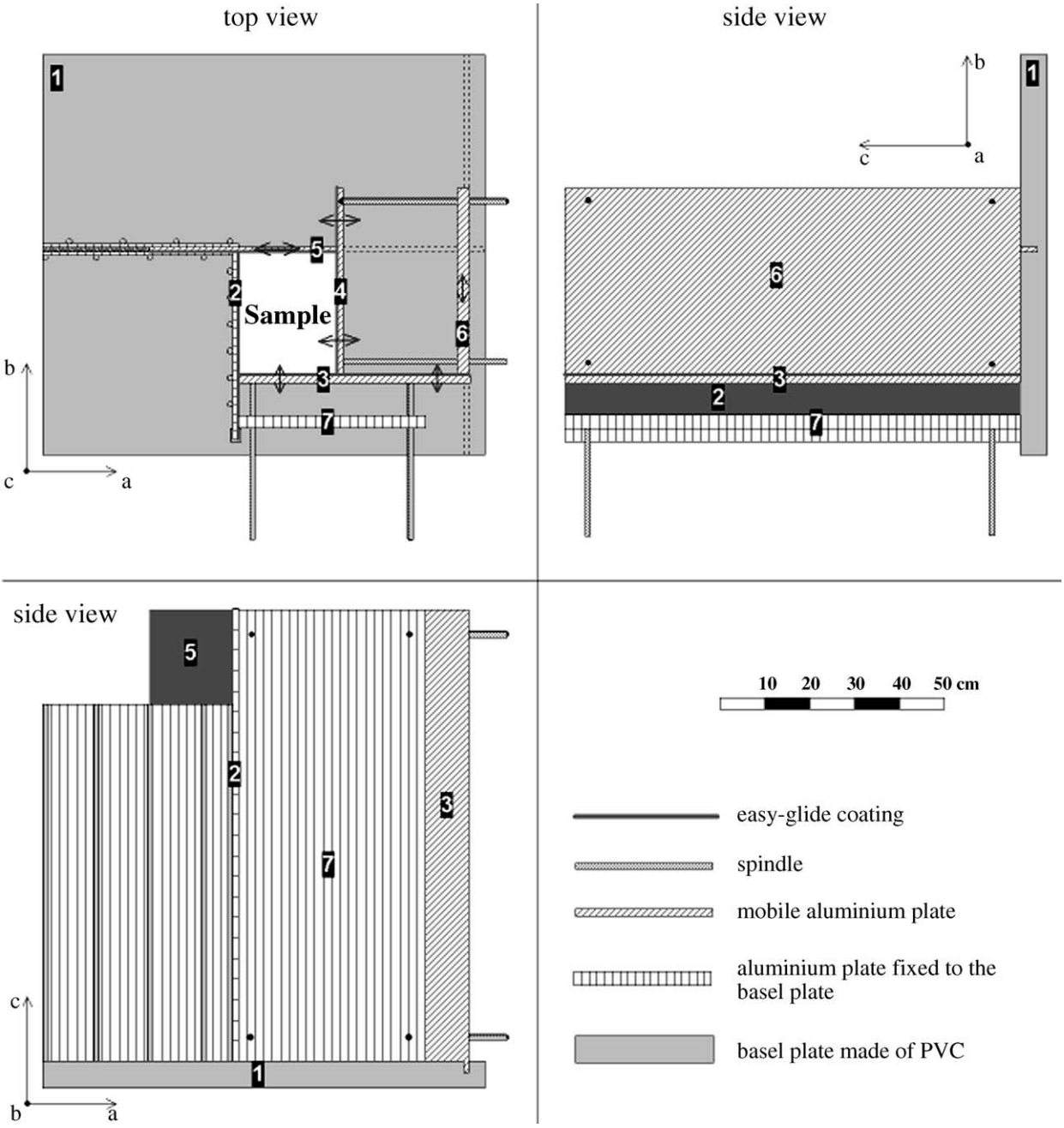

Fig. 1. Technical drawing of the new deformation apparatus, with the motors and tooth belts not shown.

are depicted in Figs. 1 and 2. The numbers in Fig. 1 refer to the bracketed numbers in the following text. The newly designed apparatus consists of a basal PVC plate [1], on which six aluminium plates [2]–[7] have been orthogonally assembled. As the initial specimen geometry leads to point loads, which result in strong bending of plates [2]–[5], these plates have been reinforced with U-shaped beams made of steel (only shown in Fig. 2).

Plates [2] and [7] are fixed to the basal plate. Plates [3]–[6] are movable. In the top view of Fig. 1 the movement direction is indicated by black arrows. Axes *a* and *b*of the orthogonal Cartesian co-ordinate system describe the horizontal directions. The *c* axis denotes the vertical direction. Plate [6] is fixed to plate [3] and slides within a groove of the basal plate along the *b* direction. Plate [5] also slides within a groove of plate [1] along the *a* direction. Except for pure flattening strain (see below), the analogue material is bounded by plates [2]–[5]. Maximum initial model dimensions are usually $30 \times 30 \times 30$ cm. To deform the specimen, the mobile plates are shifted horizontally along the basal plate in the *a* and *b* direction, respectively. Plates [2]–[5] are faced with teflon sheets to reduce friction. The movement of plates [3] and [4] is performed in each case by four spindles, driven by two motors via gears and a toothed belt

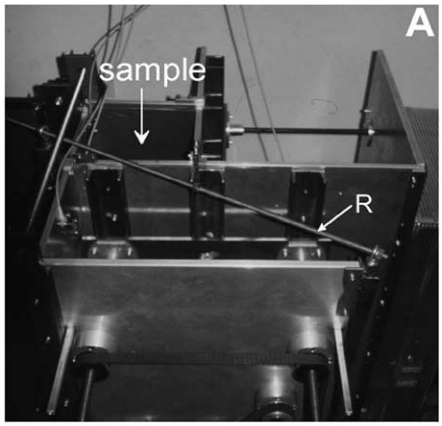

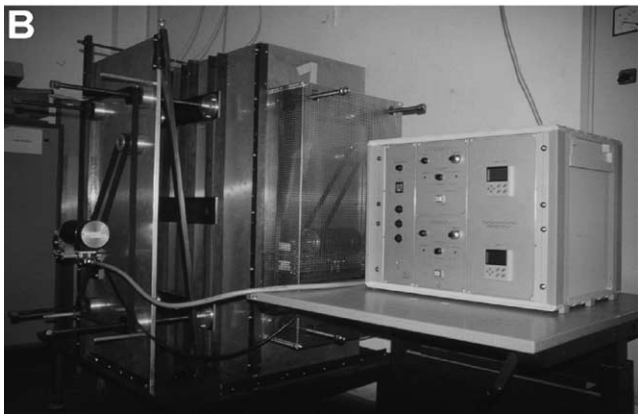

Fig. 2. Photographs of the deformation apparatus and electronic control unit. (A) view from above. (B) side view. R = reinforcement spindle.

(shown in Fig. 2 only). One of the motors is fixed to plate [7], the other is fixed to plate [6]. The rated power of the motors is 0.37 kW. The torque of the drive is 32 Nm. The motor speed is variable in the range 1–3000 rpm, and the number of revolutions are shown on a digital display. The corresponding longitudinal finite strain rates $\dot{e}$ range from 4×10^{-6} to 1×10^{-2} s^{-1}.

If plate [3] moves along the *b* direction, plates [6] and [4] also move in this direction, because plate [6] is fixed to plate [3], and plate [4] is linked with plate [6] by the four spindles. If these spindles are pushing plate [4] along the *a* direction, plate [5] is also shifted along the *a* direction. With this geometry an absolute maximum of 78% horizontal shortening is possible in the *a* and *b* directions. In cases of *pure constrictional strain* (Flinn parameter $k = \infty$) a control gear maintains the same speed for both motors, meaning that plates [3] and [4] are moving with the same velocity along the horizontal $Y = Z$ axis of the finite strain ellipsoid, and the *X* axis is vertical. There are two possibilities to produce *plane strain*($k = 1$). In one case, plate [3] and associated plates [4] and [6] move parallel to the *b* direction (that is equivalent to the *Z* axis of the finite strain ellipsoid), whereas plate [5] is immobile. In the other case, plates [3] and [6] are immobile and plates [4] and [5] move along the *a* direction that is parallel to the *Z* axis of the finite strain ellipsoid. Similar to the case of constrictional strain, the *X* axis of the finite strain ellipsoid is vertical in both cases of plane strain configuration. There are also two possibilities for *pure flattening strain*($k = 0$). If enough space is initially present between the specimen and plates [2] and [4], we can push plate [3] along the *b* direction that is parallel to the *Z* axis of the finite strain ellipsoid. In this case, the equal *X* and *Y* axes of the finite strain ellipsoid are vertical and horizontal (parallel to the *c* and *a* direction in Fig. 1a), respectively. In cases where enough space is present between the specimen and plates [3] and [5], we can move plate [4] along the *a* direction (that is parallel to *Z*) to produce pure flattening strain.

3. Three-dimensional coaxial deformation of rheologically stratified material

As a first step, the new apparatus has been used for deforming rheologically stratified analogue material to produce folds and boudins under oblate, plane and constrictional conditions. The structures that could possibly develop within these deformation regimes are depicted in the schematic drawings of Fig. 3 (see also Weijermars, 1997). As noted above, most experiments found in the literature were carried out under *plane strain conditions*, where the layer is oriented either perpendicular to the long axis *X* or perpendicular to the short axis *Z* of the finite strain ellipsoid. Simple folds, mullions, boudins and inverse folds should develop under these conditions (Fig. 3a–d). Only a few experiments have considered the situation where the layer is oriented perpendicular to the intermediate *Y* axis of the finite strain ellipsoid under plane strain (Fig. 3e and f). This arrangement should result in folds with axes parallel to the long axis *X* of the finite strain ellipsoid (Watkinson, 1975; Grujic and Mancktelow, 1995).

Moreover, the structures developed within the *constrictional regime*are largely unknown. In this case folds and boudins should develop simultaneously if a stiff layer is embedded in a weaker matrix with the *X* axis parallel to the layer (Fig. 3g and i; Fletcher, 1995; Kobberger and Zulauf, 1995). If, on the other hand, a weak layer is embedded in a stiff matrix, mullions and inverse folds should develop simultaneously (Fig. 3h and j). If the stiff (weak) layer is oriented perpendicular to the *X* axis of the finite strain ellipsoid, constriction should lead to dome and basin folds and mullions (Fig. 3k and l).

Apart from chocolate tablet boudinage (Fig. 3o), results of experimental deformation are also largely lacking in the *pure flattening field*. Simultaneous growth of folds (mullions) and boudins (inverse folds) may also occur under pure flattening strain if the layer is oriented parallel to the *Z* axis of the finite strain ellipsoid (Fig. 3m and n, q and r).

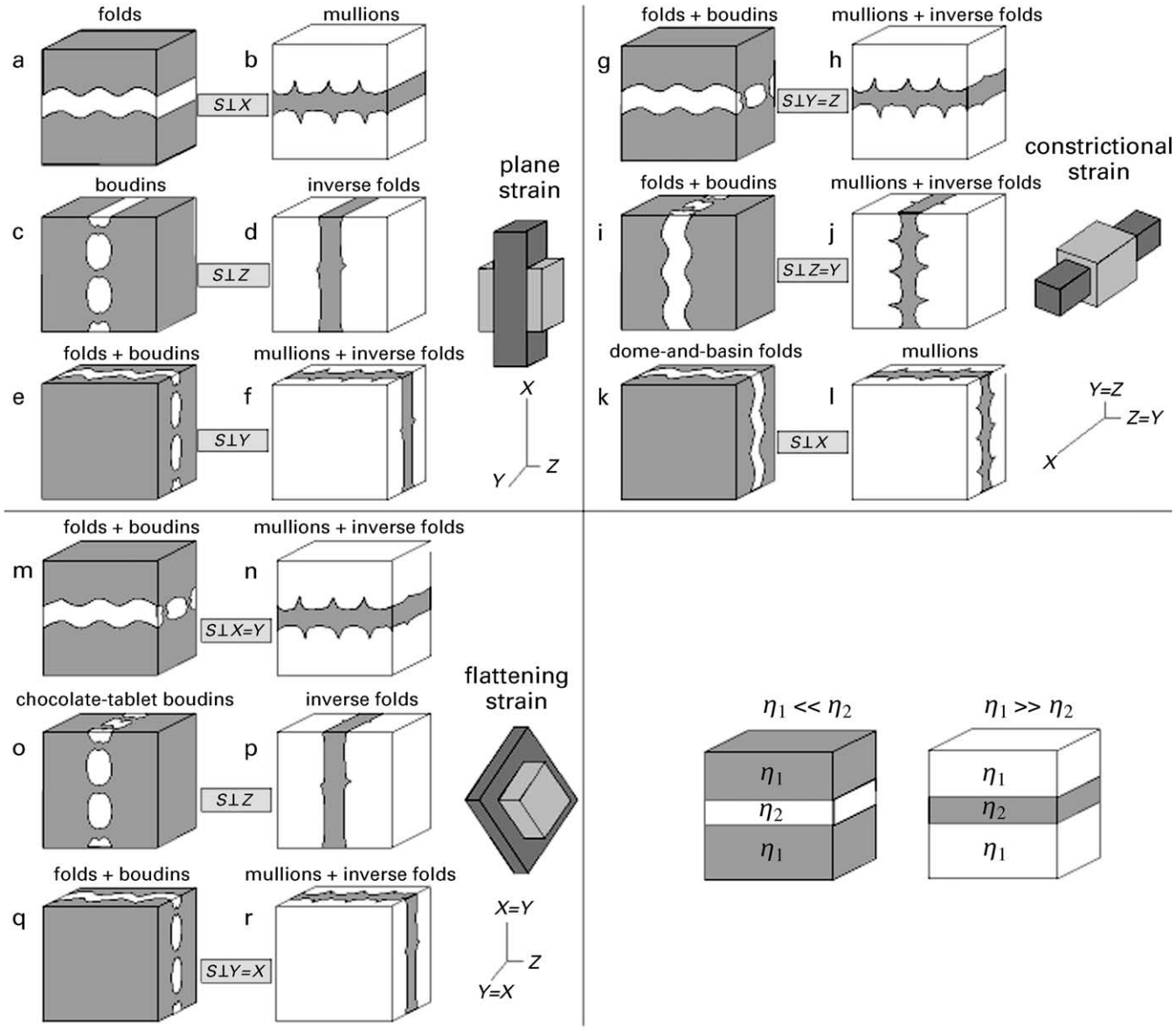

Fig. 3. Schematic drawings of three-dimensional coaxial deformation of a stiff layer embedded in a weak matrix and vice versa. S = layer; $X > Y > Z$ = principal axes of finite strain ellipsoid; η = apparent viscosity.

4. First experiments with rheologically stratified plasticine

4.1. Experimental procedure

To demonstrate the impact of the different deformation regimes on the deformation structures of rheologically stratified analogue material, we investigated a stiff layer, with viscosity η_2 and stress exponent n_2, embedded in a weak matrix, with viscosity η_1 and stress exponent n_1. The following seven deformation regimes were considered: (1) plane strain with the layer perpendicular to the long axis of the finite strain ellipsoid (Fig. 3a), (2) plane strain with the layer perpendicular to the intermediate axis of the finite strain ellipsoid (Fig. 3e), (3) plane strain with the layer perpendicular to the short axis of the finite strain ellipsoid (Fig. 3c), (4) pure flattening with the layer parallel to the short axis of the finite strain ellipsoid (Fig. 3m and q), (5) pure flattening with the layer perpendicular to the short axis of the finite strain ellipsoid (Fig. 3o), (6) pure constriction with the layer parallel to the long axis of the finite strain ellipsoid (Fig. 3g and i), and (7) pure constriction with the layer perpendicular to the long axis of the finite strain ellipsoid (Fig. 3k).

The undeformed specimens (matrix plus layer) were cubes with edge lengths ranging from 100 to 200 mm. Both the layer and the matrix were produced by cutting large blocks of undeformed plasticine with a special wire saw. Distinct instabilities were not inserted into the layer before assembling it with the matrix blocks. Before putting

Table 1
Boundary conditions for experimental runs. C_1 = material constant of matrix plasticine; C_2 = material constant of stiff layer; η_1 = matrix viscosity at 10% strain, a strain rate of 4×10^{-3} s^{-1} and a temperature of $T = 25$ °C; η_2 = layer viscosity under same conditions; m = viscosity contrast (η_2/η_1); H_i = initial layer thickness; H_f = final layer thickness. The analogue material used for viscosity contrast $m = 4.6$ is as follows: matrix—*Beck's orange* plasticine with 100 ml oil kg^{-1}; layer—*Kolb brown* plasticine with 50 ml oil kg^{-1}. The analogue material used for the viscosity contrast $m = 9.7$ is as follows: matrix—*Beck's orange* plasticine with 75 ml oil kg^{-1}; layer—*Kolb brown* plasticine

Run nr.:	H_i (mm)	H_f (mm)		η_1 (matrix) (Pa s)	η_2 (layer) (Pa s)	m	n_1 (matrix)	n_2 (layer)	C_1 (matrix) (MPa^{-n} s^{-1})	C_2 (layer) (MPa^{-n} s^{-1})	Layer thickening H_f/H_i in %		Structures
Plane strain (S perpendicular to X)	1.7	3.1	± 0.3	2.06×10^6	9.40×10^6	4.6	7.2	7.0	2.23×10^{10}	3.26×10^5	81	± 20	Folds
Plane strain (S perpendicular to Z)	1.7	1.3	± 0.2	2.06×10^6	9.40×10^6	4.6	7.2	7.0	2.23×10^{10}	3.26×10^5	− 20	± 14	Boudins
Plane strain (S perpendicular to Y)	1.8	2.3	± 0.5	2.06×10^6	9.40×10^6	4.6	7.2	7.0	2.23×10^{10}	3.26×10^5	32	± 18	?Folds + boudins
Pure flattening (S perpendicular to $X = Y$)	1.8	3.2	± 0.4	2.06×10^6	9.40×10^6	4.6	7.2	7.0	2.23×10^{10}	3.26×10^5	74	± 20	Folds + boudins
Pure flattening (S perpendicular to Z)	1.8	1.7	± 0.2	2.06×10^6	9.40×10^6	4.6	7.2	7.0	2.23×10^{10}	3.26×10^5	− 8	± 13	Boudins
Pure constriction (S perpendicular to X)	1.7	3.8	± 0.7	2.06×10^6	9.40×10^6	4.6	7.2	7.0	2.23×10^{10}	3.26×10^5	122	± 16	Folds
(1) Pure constriction (S perpendicular to $Y = Z$)	1.9	2.0	± 0.5	2.06×10^6	9.40×10^6	4.6	7.2	7.0	2.23×10^{10}	3.26×10^5	7	± 27	Boudins
(2) Pure constriction (S perpendicular to $Y = Z$)	3.4	3.8	± 0.3	2.29×10^6	2.23×10^7	9.7	9.1	5.8	2.11×10^{13}	2.27×10^2	10	± 9	Folds + boudins

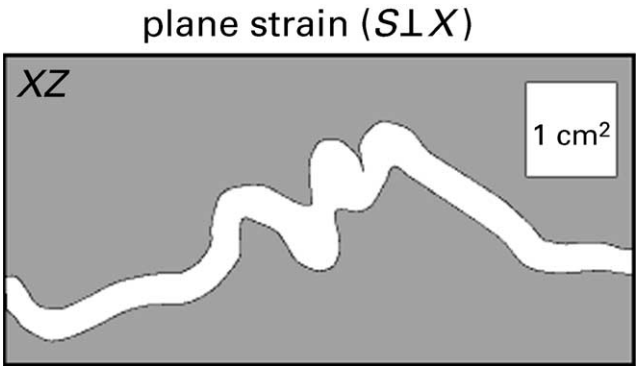

Fig. 4. *XZ* section showing folding of the stiff layer under plane strain conditions with the layer initially perpendicular to the long axis of the finite strain ellipsoid ($S \top X$).

the specimen into the machine, its sides were lubricated with vaseline and put into a bag made of ultrathin PVC to reduce friction. Subsequently the bag was also lubricated with vaseline and then the specimen was fixed between the plates within the machine. The initial thickness of the stiff layer varied between 1.6 and 1.9 mm. Only in one single case of pure constricion, the layer thickness was set at 3.4 mm. The layer consisted of dark brown plasticine, produced by the company *Kolb* in Hengersberg, Germany. The matrix was made of orange plasticine, made by the company *Beck's Plastilin* in Gomaringen, Germany. To change its viscosity, the original plasticine was partly modified by mixing it with pharmaceutical white oil (liquid paraffin). 50 and 100 ml oil kg^{-1} were added to *Kolb brown* and to *Beck's orange* plasticine, respectively. In one specific constrictional run we used the original unmodified *Kolb brown* plasticine for the stiff layer, which was embedded in *Beck's orange* plasticine, mixed with 75 ml oil per kg. Table 1 shows the layer thickness and the rheological data of the plasticine. Apart from viscosity η and stress exponent n, the viscosity ratio m between layer and matrix, and the material constant C of the viscous flow law

$$\dot{e} = C\sigma^n \tag{1}$$

are listed for the different runs (σ is the stress difference). All these data have been derived from stress versus strain plots based on constant strain rate uniaxial compression tests, the latter carried out with a biaxial shear apparatus (Zwick/Z050). More details about the analytical procedure and rheological data will be published elsewhere.

Each experimental run was conducted at a longitudinal strain rate $\dot{e}_Z$ of 4×10^{-3} s^{-1} until a finite longitudinal strain of $e_Z = -0.5$ was reached along the short axis of the finite strain ellipsoid. Only in one case of pure constriction was the finite strain along the $Y = Z$ axis equal to -0.3 at the end of the experiment. Constant motor velocity does not yield a constant incremental strain rate $\dot{e}_i$. The latter is related to the finite strain rate $\dot{e}_f$ by the equation

$$\dot{e}_i = \dot{e}_f / S \tag{2}$$

where S is the stretch. This effect is small at low strains. In our experiments the finite longitudinal strain is at most 50%, resulting in a maximum difference between $\dot{e}_f$ and $\dot{e}_i$ of 1.1 s^{-1} that can be neglected.

To investigate the geometry of the deformed stiff layer, the specimen was cut with a tense wire (wire saw) parallel to the principal planes of the finite strain ellipsoid. In cases where boudins and folds developed simultaneously, the specimen was first cut in half along the X axis. One of the halves served for analysing the geometry of the boudins, the other half was used to examine the folds. The spacing of the single cuts was set at 1–3 cm. There was no problem in reassembling the *YZ* sections in order to investigate the *XZ* sections. In addition, we used computer tomography (CT) in cases where the newly formed structures were weakly developed and thus difficult to examine using the procedure described above. The CT-studies were performed on a multislice spiral CT-scanner (Somatom Plus 4, Volume Zoom, Siemens Erlangen). The modulation of the scans was carried out using the following conditions: collimation 4×1 mm; slice 1.25 mm; increment 1 mm, and table feed 8.7 mm. According to details reported by the manufacturer and X-ray diffraction analyses, the brown plasticine of the stiff layer contains barite as filler material, whereas the orange plasticine includes potato starch and is free from barite. As a result, the X-ray contrast was sufficient to distinguish layer and matrix in CT-images.

The first seven experiments were carried out with a viscosity ratio m of 4.6 between matrix (*Beck's orange* plasticine with 100 ml oil kg^{-1}) and layer (*Kolb brown* plasticine with 50 ml oil kg^{-1}). At a finite strain e_Z of 10% and a strain rate $\dot{e}_Z$ of 4×10^{-3} s^{-1}, the apparent viscosity and stress exponent for matrix and layer are 2.1×10^6 Pa s and 7.2, respectively, and 9.4×10^6 Pa s and 7.0, respectively. The last experiment was performed with a viscosity ratio of $m = 9.7$ between matrix (*Beck's orange* plasticine with 75 ml oil kg^{-1}) and layer (original *Kolb brown* plasticine). At a finite strain of 10% and a strain rate of 4×10^{-3} s^{-1} the apparent viscosity and stress exponent for matrix and layer are 2.3×10^6 Pa s and 9.1, respectively, and 2.2×10^7 Pa s and 5.8, respectively. *Beck's orange* plasticine (with and without oil) shows steady-state behaviour after ca. 5% strain. The original *Kolb brown* plasticine shows weak strain hardening, even at higher strain magnitudes. The effect of strain hardening, however, is significantly reduced when adding oil to *Kolb brown* plasticine.

The thickness of the deformed layers was determined by multiple measurements carried out in several sections. The average values and standard deviation listed in Table 1 result from these measurements. In cases of pinch-and-swell and boudinage structures, we measured only the thickest part of the swell or boudin, respectively.

4.2. Results

Classical *plane strain folding,* with the stiff layer oriented

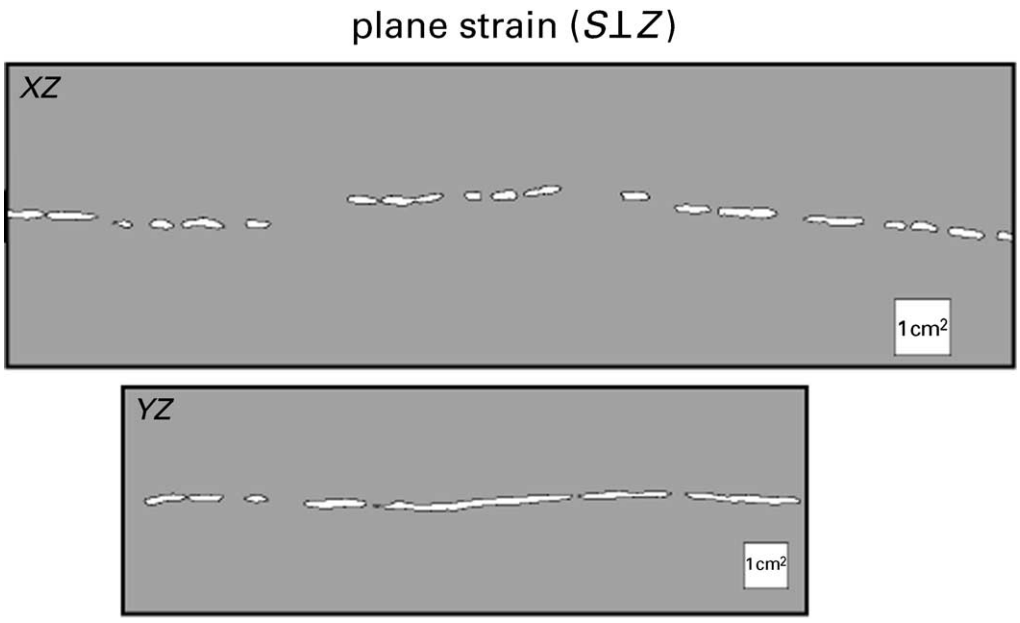

Fig. 5. *XZ* and *YZ* section showing boudinage and 'pseudo-boudins' of the stiff layer, respectively, under plane strain with the layer initially perpendicular to the short axis and parallel to the long axis of the finite strain ellipsoid.

perpendicular to the long axis of the finite strain ellipsoid ($S \top X$; Fig. 3a), results in 81 ± 20% layer thickening and striking folds in the *XZ* section of the finite strain ellipsoid (Fig. 4). These structures are according to our expectations.

In the second case of *plane strain* deformation, with the layer oriented perpendicular to the short axis of the finite strain ellipsoid ($S \top Z$; Fig. 3c), layer thinning has been determined at 20 ± 14%. This section shows the expected pinch-and-swell and boudinage structures (Fig. 5). The *YZ* sections show in a few cuts only 'pseudo-boudins', the latter resulting from the fact that some boudin long axes are oblique with respect to the principal strain axes (see below).

In the third case of *plane strain* deformation, with the layer now oriented perpendicular to the intermediate *Y* axis of the finite strain ellipsoid ($S \top Y$; Fig. 3e), layer thickening has been determined at 32 ± 18%. Moreover, the layer shows pinch-and-swell as well as boudinage structures in the *XZ* sections, whereas the *YZ* sections are almost free of structures. Only a few of them show weak low-amplitude/high-wavelength folding (Fig. 6). This is also obvious from the CT-image (Fig. 7). It is clear from this image that the necks between the boudins frequently deviate from the *YZ* section of the finite strain ellipsoid. This oblique orientation, with respect to the principal strain axes, explains why in some *YZ* sections the stiff layer shows occasional fractures, which are referred to as 'pseudo-boudinage'.

Pure flattening with the stiff layer oriented parallel to the short axis of the finite strain ellipsoid ($S \top X = Y$; Fig. 3m and q) led to folds in the $XZ = YZ$ sections, whereas the *XY* sections show incipient boudinage (Fig. 8). Layer thickening has been determined at 74 ± 20%.

In the second case of *pure flattening* deformation, with the layer perpendicular to the short axis of the finite strain ellipsoid ($S \top Z$; Fig. 3o), chocolate tablet boudinage developed. In this case, the layer thickness did not significantly change (−8 ± 13%). Apart from boudinage, there is evidence for pinch-and-swell structures (Fig. 9).

Under *pure constriction*, with the stiff layer oriented

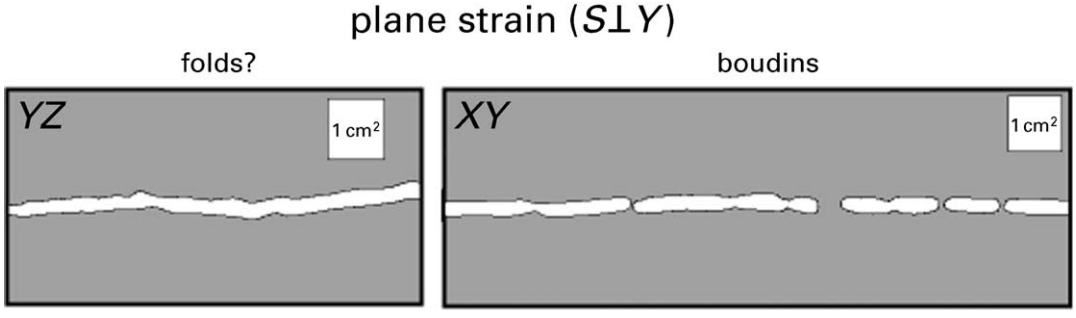

Fig. 6. *YZ* and *XY* section showing possible weak folding and well developed boudinage of the stiff layer under plane strain conditions, with the layer initially perpendicular to the intermediate axis and the fold axis parallel to the long axis of the finite strain ellipsoid ($S \top Y$).

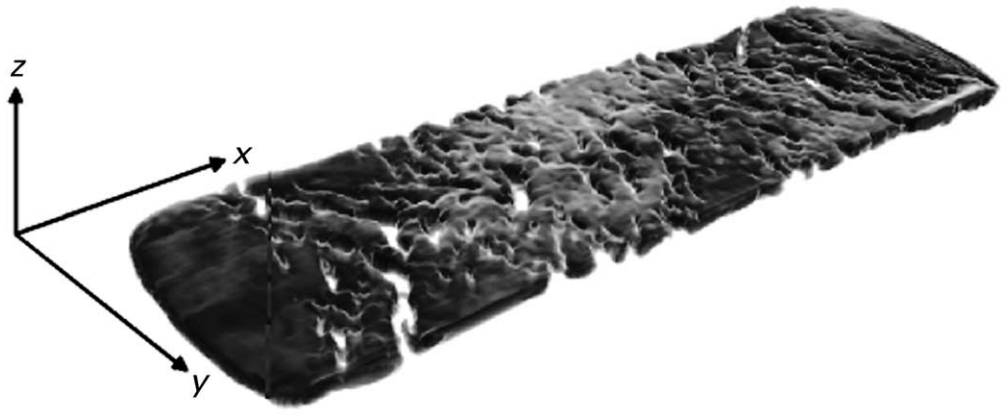

Fig. 7. Three-dimensional view of boudinaged stiff layer based on computer tomography (CT). Note the oblique orientation of the necks with respect to the principal strain axes. Same deformation regime as in Fig. 6.

perpendicular to the long axis of the finite strain ellipsoid ($S \top X$; Fig. 3k), dome and basin folds developed (Fig. 10). The layer thickening has been determined at 122 ± 16%.

Under *pure constriction*, with the layer oriented parallel to the X axis of the finite strain ellipsoid ($S \top Y = Z$; Fig. 3g and i), the layer shows boudinage in $XZ = XY$sections (Fig. 11). The YZ sections are free from folding, but show weak 'pseudo-boudinage'. Similar to the plane strain deformation described above, with $S \top Y$, this 'pseudo-boudinage' results from the fact that some of the necks do not follow the YZ plane, but are slightly oblique with respect to the principal strain axes. Layer thickening has been determined at 7 ± 27%.

To examine whether simultaneous folding and boudinage is generally possible under pure constriction (cf. Kobberger and Zulauf, 1995), we carried out a second run using other types of plasticine that result in a higher viscosity ratio of $m = 9.7$ (for further details see Table 1). Apart from varying the rheological parameters, the initial layer thickness was increased to 3.4 mm. Under these conditions boudins developed in $XZ = XY$ sections, whereas weak but distinct folding appears in YZ sections (Fig. 12). This folding does not occur in all sections, suggesting that the fold axis is not constant in orientation. This is also obvious from CT-images (Fig. 13). Thickening of the stiff layer has been determined at 10 ± 9% that is similar low as in the first case of pure constriction.

5. Discussion

The new deformation apparatus is able to produce three-dimensional coaxial deformation covering the full range from pure flattening to pure constriction. Although friction between the walls of the machine and the specimen has been reduced by double coated sheets of vaseline, there are still boundary effects, such as drag of the layer along the walls (e.g. Figs. 10 and 11). As these features are largely restricted to the outer margins of the specimens, they can largely be ignored when making statistical geometrical analysis of the deformed structures.

Given that the boundary conditions like temperature, stress exponent, and viscosity ratio between layer and matrix do not significantly change from one experiment to the other, the deformation geometry of the stiff layer is strongly controlled by the magnitude of finite strain and

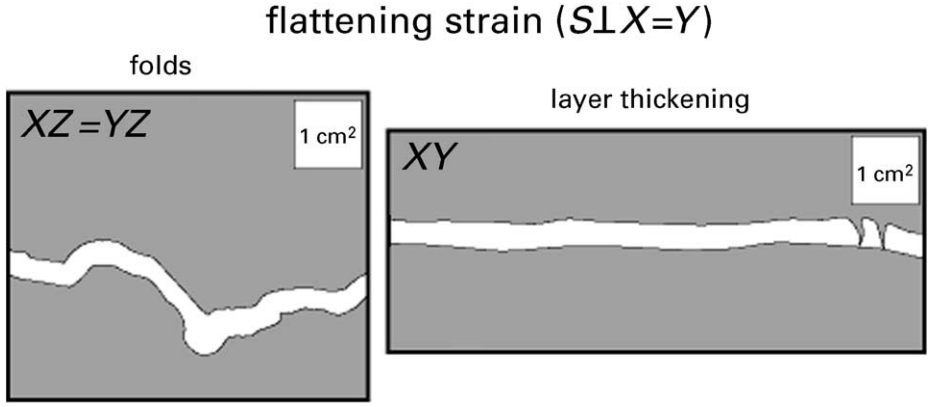

Fig. 8. $YZ = XZ$ and XY section showing folding and incipient boudinage of the stiff layer, respectively, under pure flattening strain with the layer initially parallel to the short axis of the finite strain ellipsoid.

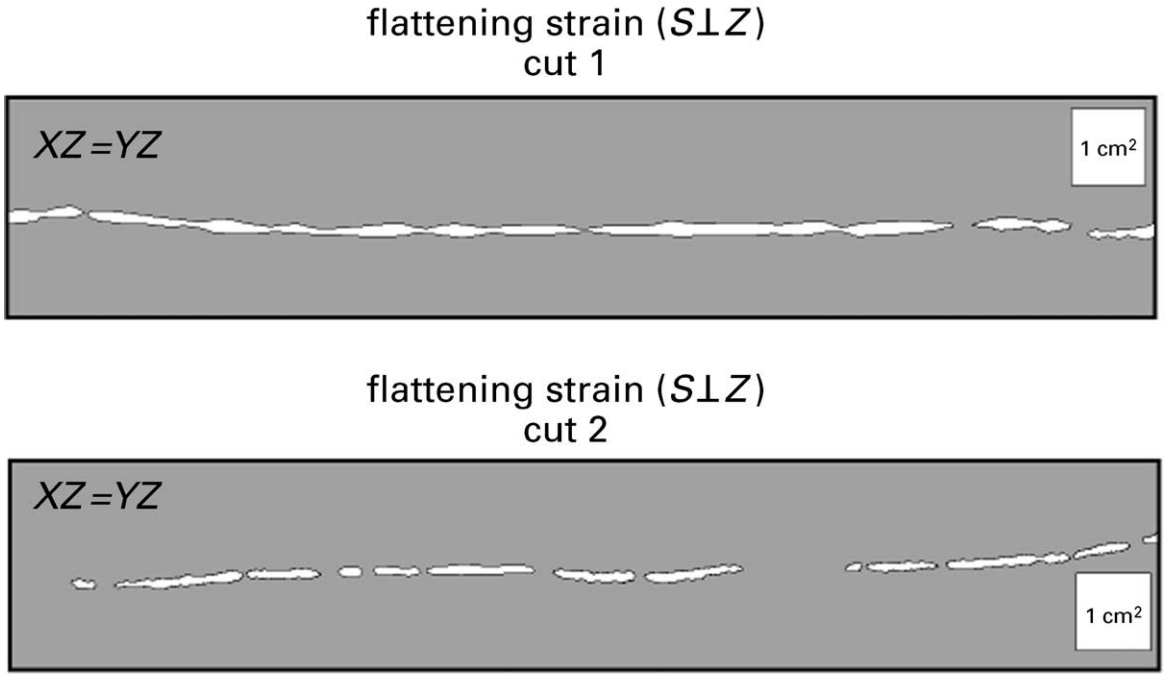

Fig. 9. $XZ = YZ$ section showing boudinage in both sections of the stiff layer under pure flattening strain with the layer initially oriented parallel to the long axis of the finite strain ellipsoid.

the type of overall three-dimensional coaxial strain. In cases where the viscosity ratio between layer and matrix is low (i.e. ca. 5), folding is most easily performed under pure flattening and plane strain conditions, the latter characterised by $S \top X$. Both folding regimes are characterised by strong layer thickening to about twice the original amount. The degree of layer thickening is much lower (less than 50%), if boudinage structures develop under plane strain with the layer oriented perpendicular to the Y axis ($S \top Y$). As there is no change in length along Y, this type of layer thickening could be explained by the different strain rates of layer and matrix along X and Z. Convergent flow of the layer along Z leads to thickening of the layer, whereas extensional flow of the layer along X causes thinning. If the flow rate of the weak matrix is similar along X and Z, but the flow rate of the layer along Z exceeds that along X, the layer will show thickening.

In cases of chocolate-tablet and plane-strain boudinage ($S \top Z$) the layer thickness does not significantly change. Maximum layer thickening, on the other hand, is associated with the development of dome and basin folds under constriction. This can be explained by the fact that the layer is radially contracted.

There is no or almost no evidence for folding of the stiff layer at a viscosity contrast of $m \cong 5$ under constriction ($S \top Y = Z$) and under plane strain ($S \top Y$), although both

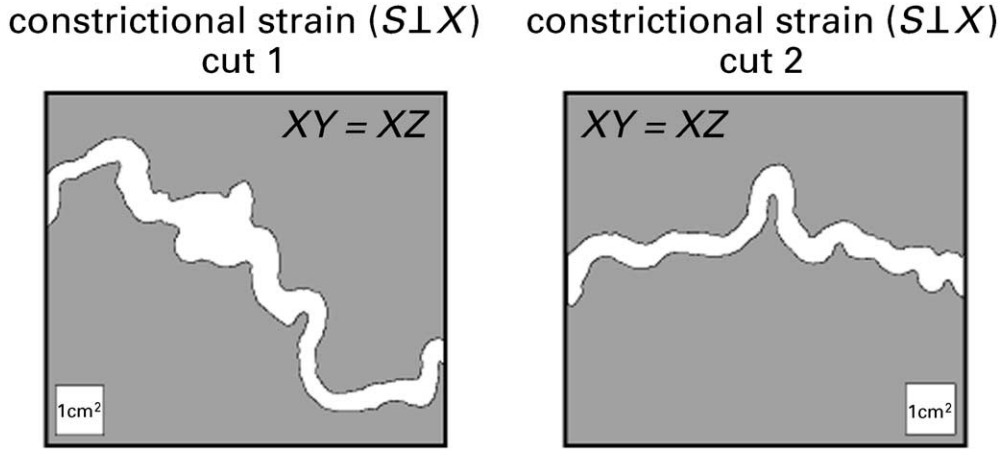

Fig. 10. $XZ = XY$ sections showing dome-and-basin folds of the stiff layer under pure flattening strain with the layer initially oriented perpendicular to the long axis of the finite strain ellipsoid.

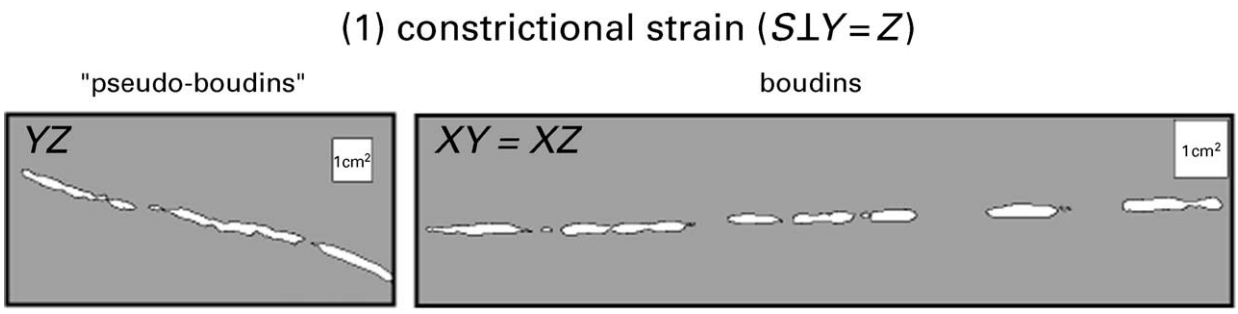

Fig. 11. *YZ* and *XY* = *XZ* section showing 'pseudo-boudinage' and boudinage of the stiff layer, respectively, under pure constrictional strain with the layer initially oriented parallel to the long axis of the finite strain ellipsoid. Viscosity contrast between stiff layer and matrix was ca. 5.

experiments led to boudinage. These observations are in line with results obtained by Neurath and Smith (1982) who investigated folding and boudinage of wax models. However, both authors explain the difference in growth rate between folds and boudins by strain softening of the wax. The influence of strain softening is much greater for necking than for folding. In our case, however, we are dealing with analogue material that either shows steady-state behaviour or strain hardening. Thus, apart from strain softening, there should be other so far unknown reasons why the growth rate of boudins exceeds that of folds under plane strain.

The simultaneous development of folds and boudins was possible during the second pure constrictional run, where the viscosity ratio between layer and matrix was about twice the previous value. Similar boundary conditions have been used by Kobberger and Zulauf (1995) to produce coeval folds and boudins under constriction. They have shown that layer thickness does not significantly change in this case, comparable with our results. As constrictional folding does not occur in all of the *YZ* sections, it is suggested that the fold axes are not constant in orientation. The reason for these irregularities in folding can be explained by the presence of boudins that affect the orientation of the fold axes and vice versa. The interaction between folds and boudins is obvious from the CT-images. Slightly oblique orientation of the boudin necks, with respect to the principal strain axes, may lead to pseudo-boudins in *YZ* sections of the finite strain ellipsoid (Fig. 13). Thus, pure constriction and plane strain, with $S \top Y$, result in complex, but characteristic, patterns of coeval folds and boudins. These patterns can be distinguished from those that result from polyphase deformation such as folding of a stiff layer that was boudinaged before.

6. Conclusions and open questions

We conclude from our first studies of three-dimensional coaxial deformation that the geometry of a deformed stiff layer, embedded in a weaker matrix, does not only depend on layer thickness and the rheology of matrix and layer, but is further significantly controlled by the type of three-dimensional bulk deformation. Simultaneous growth of folds and boudins is possible under constriction and plane strain with $S \top Y$, but needs particular boundary conditions. Similar results have been obtained by Fletcher (1995), who theoretically investigated the three-dimensional folding and necking of a power-law layer. Fletcher (1995) states that simultaneous growth of folds and pinch-and-swell structures, both at right angles, is not completely impossible, but rather difficult.

Our observations are of major interest for the interpretation of natural examples. In cases where rheologically

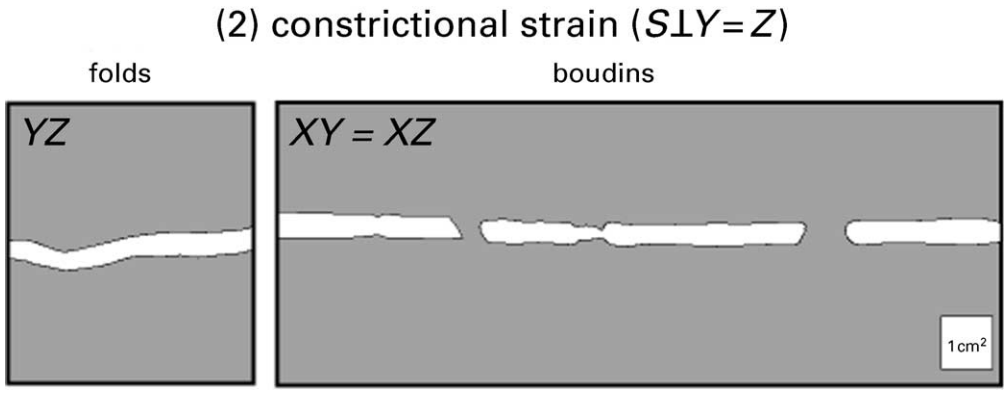

Fig. 12. *YZ* and *XY* = *XZ* section showing low amplitude/large wavelength folds and boudins of the stiff layer, respectively, under pure constrictional strain with the layer initially oriented parallel to the long axis of the finite strain ellipsoid. Viscosity contrast was ca. 10.

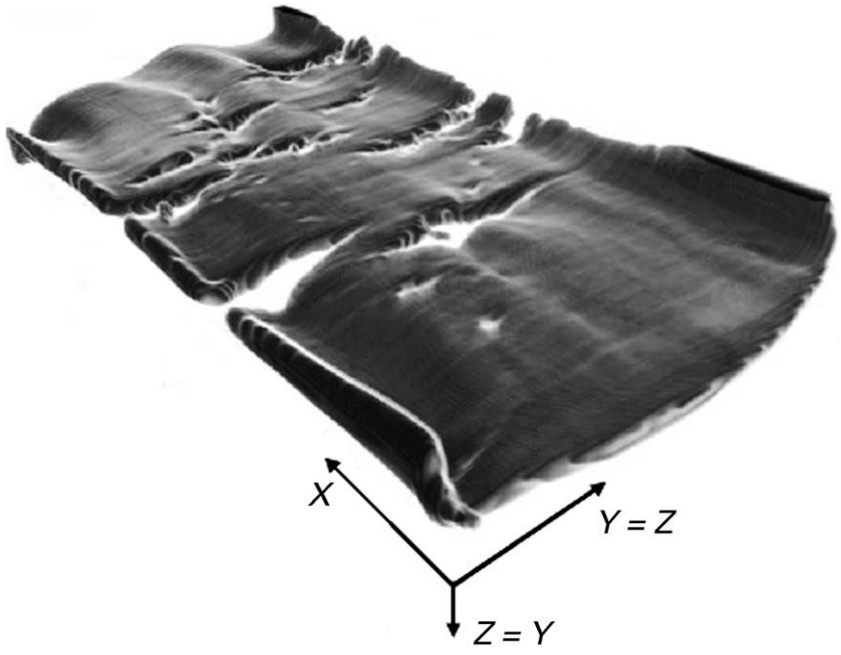

Fig. 13. Three-dimensional view of folds and boudins based on computer tomography (CT). Note that boudins are affecting the geometry of folds and vice versa. Same deformation regime and conditions as in Fig. 12.

stratified natural rocks have been deformed under non-plane coaxial conditions, the relation between geometry (e.g. fold wavelength, layer thickness) and rheology (e.g. viscosity contrast between layer and matrix, stress exponent) cannot be explained by equations which hold for plane strain (Ramberg, 1960; Biot, 1961; Fletcher, 1974; Smith, 1977). This conclusion is in line with Fletcher (1995) who concludes that "good estimates of rheological model parameters are best carried out for cases in which the bulk strain is nearly plane".

There are several open questions that will be answered by further experiments. They concern not only the influence of varying viscosity contrast and layer thickness, but also the impact of varying stress exponents, strain rates, and orientation of the layer. Further studies will also focus on three-dimensional coaxial deformation of a weak layer that is surrounded by a stiff matrix to produce mullions and inverse folds.

Acknowledgements

We are grateful to H. Schmeling (University of Frankfurt) for his helpful comments when designing the apparatus. Visualisation of CT images were carried out with a software tool developed from the Computer Graphics Group at the Technical Faculty of the University of Erlangen. Thanks also to P.R. Cobbold and N. Mancktelow for their constructive reviews. This study was supported by Deutsche Forschungsgemeinschaft [Zu 73/7-1] which is gratefully acknowledged.

References

Abbassi, M.R., Mancktelow, N.S., 1992. Single layer buckle folding in non-linear materials-I. Experimental study of fold development from an isolated initial perturbation. Journal of Structural Geology 14, 85–104.

Biot, M.A., 1961. Theory of folding of stratified viscoelastic media and its implications in tectonics and orogenesis. Geological Society of America Bulletin 72, 1595–1620.

Cobbold, P.R., 1975a. A biaxial press for model deformation and rheological tests. Tectonophysics 26, T1–T5.

Cobbold, P.R., 1975b. Fold propagation in single embedded layers. Tectonophysics 27, 333–351.

Fletcher, R.C., 1974. Wavelength selection in the folding of a single layer with power-law rheology. American Journal of Science 274, 1029–1043.

Fletcher, R.C., 1995. Three-dimensional folding and necking of a power-law layer: are folds cylindrical, and, if so, do we understand why? Tectonophysics 247, 65–83.

Gapais, D., Fiquet, G., Cobbold, P.R., 1991. Slip system domains, 3. New insights in fault kinematics from plane-strain sandbox experiments. Tectonophysics 188, 143–157.

Grujic, D., Mancktelow, N.S., 1995. Folds with axes parallel to the extension direction: an experimental study. Journal of Structural Geology 17, 279–291.

Hudleston, P.J., 1973. An analysis of single layer folds developed experimentally in viscous media. Tectonophysics 16, 189–214.

Kidan, T.W., Cosgrove, J.W., 1996. The deformation of multilayers by layer-normal compression; an experimental investigation. Journal of Structural Geology 18, 461–474.

Kobberger, G., Zulauf, G., 1995. Experimental folding and boudinage under pure constrictional conditions. Journal of Structural Geology 17, 1055–1063.

Mancktelow, N.S., 1988. An automated machine for pure shear deformation of analogueue materials in plane strain. Journal of Structural Geology 10, 101–108.

Mandal, N., Khan, D., 1991. Rotation, offset and separation of oblique-fracture (rhombic) boudins: theory and experiments under layer-normal compression. Journal of Structural Geology 13, 349–356.

Neurath, C., Smith, R.B., 1982. The effect of material properties on growth-rates of folding and boudinage: experiments with wax models. Journal of Structural Geology 4, 215–229.

Pfiffner, O.A., Ramsay, J.G., 1982. Constraints on geological strain rates: arguments from finite strain states of naturally deformed rocks. Journal of Geophysical Research 87, 311–321.

Ramberg, H., 1955. Natural and experimental boudinage and pinch-and-swell structures. Journal of Geology 63, 512–526.

Ramberg, H., 1960. Relationships between lengths of arc and thickness of ptygmatically folded veins. American Journal of Science 258, 36–46.

Ramberg, H., 1961. Contact strain and folding instability of a multilayered body under compression. Geologische Rundschau 51, 405–439.

Smith, R.B., 1977. Formation of folds, boudinage, and mullions in non-Newtonian materials. Geological Society of America Bulletin 88, 312–320.

Sokoutis, D., 1990. Experimental mullions at single and double interfaces. Journal of Structural Geology 12, 365–373.

Strömgård, K.E., 1973. Stress distribution during deformation of boudinage and pressure shadows. Tectonophysics 16, 215–248.

Watkinson, A.J., 1975. Multilayer folds initiated in bulk plane strain, with the axis of no change perpendicular to the layering. Tectonophysics 28, T7–T11.

Weijermars, R., 1997. Principles of Rock Mechanics. Alboran Science Publishing, 359pp.

Williams, P.F., Jiang, D., 2001. The role of initial perturbations in the development of folds in a rock-analogue. Journal of Structural Geology 23, 845–856.